

Fate of clumps in damped Ly α systems

Ilian T. Iliev,^{1*} Hiroyuki Hirashita² and Andrea Ferrara³

¹ *Canadian Institute for Theoretical Astrophysics, University of Toronto, 60 St. George Street, Toronto, ON M5S 3H8, Canada*

² *Center for Computational Sciences, University of Tsukuba, Tsukuba 305-8577, Japan*

³ *SISSA/International School for Advanced Studies, Via Beirut 4, 34014 Trieste, Italy*

24 March 2018

ABSTRACT

Recent observations have revealed that damped Ly α clouds (DLAs) host star formation activity. In order to examine if such star formation activity can be triggered by ionization fronts, we perform high-resolution hydrodynamics and radiative transfer simulations of the effect of radiative feedback from propagating ionization fronts on high-density clumps. We examine two sources of ultraviolet (*UV*) radiation field to which high-redshift ($z \sim 3$) galaxies could be exposed: one corresponding to the *UV* radiation originating from stars within the DLA, itself, and the other corresponding to the *UV* background radiation. We find that, for larger clouds, the propagating I-fronts created by local stellar sources can trigger cooling instability and collapse of significant part, up to 85%, of the cloud, creating conditions for star formation in a timescale of a few Myr. The passage of the I-front also triggers collapse of smaller clumps (with radii below ~ 4 pc), but in these cases the resulting cold and dense gas does not reach conditions conducive to star formation. Assuming that 85% of the gas initially in the clump is converted into stars, we obtain a star formation rate of $\sim 0.25 M_{\odot} \text{ yr}^{-1} \text{ kpc}^{-2}$. This is somewhat higher than the value derived from recent observations. On the other hand, the background *UV* radiation which has harder spectrum fails to trigger cooling and collapse. Instead, the hard photons which have long mean-free-path heat the dense clumps, which as a result expand and essentially dissolve in the ambient medium. Therefore, the star formation activity in DLAs is strongly regulated by the radiative feedback, both from the external *UV* background and internal stellar sources and we predict quiescent evolution of DLAs (not starburst-like evolution).

Key words: hydrodynamics— radiative transfer— methods: numerical — ISM: molecules — galaxies: evolution — quasar absorption lines

1 INTRODUCTION

Damped Ly α clouds are quasar (QSO) absorption line systems whose neutral hydrogen column density is larger than $\sim 2 \times 10^{20} \text{ cm}^{-2}$ (e.g. Prochaska & Wolfe 2002). This class of objects dominates the neutral hydrogen content around $z \sim 3$ and possibly also at higher and lower redshifts (e.g. Péroux et al. 2003). Because QSOs are generally luminous, DLAs provide us with unique opportunities to trace high-redshift (high- z) galaxy evolution. In particular, by identifying absorption lines of various species, the physical condition of the interstellar medium (ISM) of DLAs has been deduced.

The detection of metal lines in DLAs demonstrates the existence of heavy elements in DLAs (e.g. Lu et al. 1996; Ledoux et al. 2003). The evolution of metal abundances in DLAs can trace the chemical enrichment history of present day galaxies. Based on this and other clues, DLAs have been suggested to be the progenitors

of nearby galaxies; the similar values of the baryonic mass density in DLAs around redshift $z \sim 2$ and the stellar mass density at $z \sim 0$ has further supported this idea (Lanzetta et al. 1995; Storrie-Lombardi & Wolfe 2000). By adopting a recently favoured Lambda cold dark matter cosmology, however, Péroux et al. (2003) showed that the comoving density of H I gas at $z \sim 2$ is smaller than the comoving stellar mass density at $z \sim 0$. Yet they emphasize that a large fraction of H I gas is contained in DLAs at $z \sim 2-3$.

The existence of heavy elements in DLAs indicates that DLAs have experienced star formation. There is also direct evidence of ongoing star formation activity from the *UV* interstellar radiation field larger than the ultraviolet background (*UVB*) intensity (Ledoux et al. 2002; Wolfe et al. 2003). Hirashita et al. (2003) have theoretically shown that there are small-scale clumps whose molecular fraction is higher than 10^{-3} in DLAs. The typical size and density of such clumps are ~ 5 pc and 30 cm^{-3} , respectively. However, it is not clear if those clouds finally collapse and form stars in *UV* radiation field. It is however crucial to address this question, as most these clumps are likely to host the most active sites of star

* e-mail: iliev@cita.utoronto.ca

formation in DLAs. Howk et al. (2005) have shown the existence of cold gas in a high- z DLA, arguing that such cold gas may work as the fuel for star formation.

The nature of DLAs is at present uncertain. They have been thought to be the progenitors of nearby large galaxies. For example, Wolfe et al. (1986) propose that DLAs are disk galaxies (see also Prochaska & Wolfe 1998). More recently, Haehnelt et al. (1998) and Ledoux et al. (1998) showed that the velocity structure can be explained by infalling subgalactic clumps in collapsing dark matter halo. At $z \sim 0$, spiral galaxies may contribute predominantly to the damped Ly α absorption (Rao & Briggs 1993), but at high redshift, various classes of objects can be observed as DLAs (Cen et al. 2003). In any scenario, small clumps can form as a result of non-linear hydrodynamical processes (Wada & Norman 2001), and it is important to know if such clumps finally lead to star formation activity.

In a previous work (Hirashita et al. 2003), we have used the 2-dimensional (2-D) code of Wada & Norman (2001) suitable for disk-like geometry, in order to follow the evolution of entire galactic disk. They stress the clumpy structure of gas, whose typical size is roughly ~ 5 pc. In this paper, we build on this by examining the fate of the resulting clumps in external UV field. For this problem, we use a 2-D axially-symmetric radiative-hydrodynamical Adaptive Mesh Refinement (AMR) code CORAL (Raga et al. 1995, 1997; Mellema et al. 1998; Shapiro, Iliev & Raga 2004; Iliev, Shapiro, & Raga 2005), which is appropriate for treating each clump.

The structure of this work is as follows. We describe our numerical methods and input parameters in § 2. In section § 3 we present and discuss our results and finally, in § 4 we give our summary and conclusions. Throughout the paper we use CGS units, unless otherwise noted.

2 METHOD

2.1 Numerical methods

We use a 2-D axially-symmetric radiative-hydrodynamical Adaptive Mesh Refinement (AMR) Eulerian code CORAL (Raga et al. 1995, 1997; Mellema et al. 1998; Shapiro, Iliev & Raga 2004; Iliev, Shapiro, & Raga 2005). The hydrodynamic equations are solved by a van Leer flux-splitting method (van Leer 1982), improved to second order accuracy by use of linear gradients within cells as described in Arthur (1991). The microphysical processes are coupled to the hydrodynamical evolution by operator-splitting, i.e. solved at each timestep and results included in the energy equation. These microphysical processes include photo- and collisional ionizations, recombinations (both radiative and dielectronic), charge exchange and transfer of ionizing radiation. The code follows the non-equilibrium chemical evolution of the ionic species of H, He, C II–VI, N I–VI, O I–VI, Ne I–VI, and S II–VI (C I and S I are assumed fully-ionized). Self-gravity is currently not included. The refinement (and de-refinement) of a given region in space is decided based on the gradients of all code variables, when the gradient is larger than a pre-defined value, the region is refined and vice-versa. We used a total of 8 levels of refinement (separated by factors of 2 in cell size). More details on I-front tracking implementation and detailed tests of the method can be found in Shapiro, Iliev & Raga (2004).

2.2 H₂ formation and destruction

For the metallicity range typical of DLAs, we can assume equilibrium between H₂ formation and destruction, because the timescale of H₂ formation and destruction is well below the dynamical timescale (Hirashita et al. 2003). We adopt the formation rate of H₂ per unit volume and time, R_{dust} , by Hollenbach & McKee (1979) (see also Hirashita et al. 2003)¹:

$$R_{\text{dust}} = 4.1 \times 10^{-17} S_{\text{d}}(T) \left(\frac{a}{0.1 \mu\text{m}} \right)^{-1} \left(\frac{\mathcal{D}}{10^{-2}} \right) \times \left(\frac{T}{100 \text{ K}} \right)^{1/2} \left(\frac{\delta}{2 \text{ g cm}^{-3}} \right) \text{ cm}^3 \text{ s}^{-1}, \quad (1)$$

where a is the radius of a grain (assumed to be spherical with a radius of $0.1 \mu\text{m}$ in this paper), \mathcal{D} is the dust-to-gas mass ratio, δ is the grain material density (assumed to be 2 g cm^{-3} in this paper), and $S_{\text{d}}(T)$ is the sticking coefficient of hydrogen atoms onto dust. The sticking coefficient is given by (Hollenbach & McKee 1979; Omukai 2000)

$$S_{\text{d}}(T) = [1 + 0.04(T + T_{\text{d}})^{0.5} + 2 \times 10^{-3}T + 8 \times 10^{-6}T^2]^{-1} \times [1 + \exp(7.5 \times 10^2(1/75 - 1/T_{\text{d}}))]^{-1}, \quad (2)$$

where T_{d} is the dust temperature. We adopt $T_{\text{d}} = 20 \text{ K}$, a typical dust temperature in equilibrium with the Galactic interstellar radiation field (ISRF) (Shibai et al. 1999). However, since the reaction rate is insensitive to the dust temperature as long as $T_{\text{d}} \lesssim 70 \text{ K}$, the following results are not affected by the dust temperature. In fact, some DLAs show ISRF strengths similar to the Galactic value (Ge & Bechtold 1997; Ledoux et al. 2002; Petitjean et al. 2002). The H₂ formation rate per unit volume is estimated by $R_1 = R_{\text{dust}} n n_{\text{H}} (1 - f_{\text{H}_2})$, where $n = 1.08 n_{\text{H}}$ is the total, hydrogen and helium number density, n_{H} is the hydrogen number density and $f_{\text{H}_2} \equiv 2n_{\text{H}_2}/n$ (n_{H_2} is the H₂ number density) is the H₂ molecule fraction.

The photodissociation rate R_{diss} is estimated by (Abel et al 1997)

$$R_{\text{diss}} = (4\pi) 1.1 \times 10^8 J_{\text{LW}} S_{\text{shield}} \text{ s}^{-1}, \quad (3)$$

where J_{LW} ($\text{erg s}^{-1} \text{ cm}^{-2} \text{ Hz}^{-1} \text{ str}^{-1}$) is the UV intensity at $h\nu = 12.87 \text{ eV}$ averaged for all the solid angle, S_{shield} is the correction factor of the reaction rate for H₂ self-shielding and dust extinction. The photodissociation rate per unit volume is then estimated by $R_2 = R_{\text{diss}} n_{\text{H}_2}$, where n_{H_2} is the number density of H₂. We adopt the correction for the H₂ self-shielding by Draine & Bertoldi (1996) (see also Hirashita & Ferrara 2002). Then, we estimate S_{shield} as

$$S_{\text{shield}} = \min \left[1, \left(\frac{N_{\text{H}_2}}{10^{14} \text{ cm}^{-2}} \right)^{-0.75} \right] e^{-\sigma_{\text{dust}} N_{\text{dust}}}, \quad (4)$$

where N_{H_2} is the column density of H₂. The last term, which is due to absorption by dust is in fact of no relevance for the parameters we assume here (Hirashita & Ferrara 2005).

The metallicity level of DLAs, $\sim 0.1 Z_{\odot}$ (Pettini et al. 1994), which is the value we assume here, implies that the dust-to-gas ratio of DLAs is typically 10% of the Galactic (Milky Way) value. In

¹ In Hirashita et al. (2003) there is a typographic error. (The results are correctly calculated.) The expression in this paper is correct and R_1 in Hirashita et al. (2003) is equal to $R_{\text{dust}} n n_{\text{H}} (1 - f_{\text{H}_2})$, where f_{H_2} is the molecular fraction.

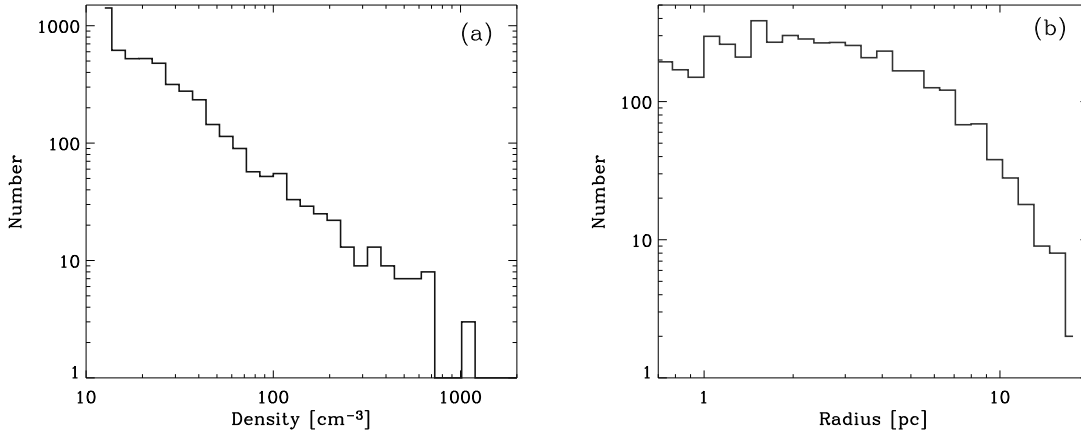


Figure 1. Distributions of clumps in disk in (a)(left) mean density and (b)(right) size.

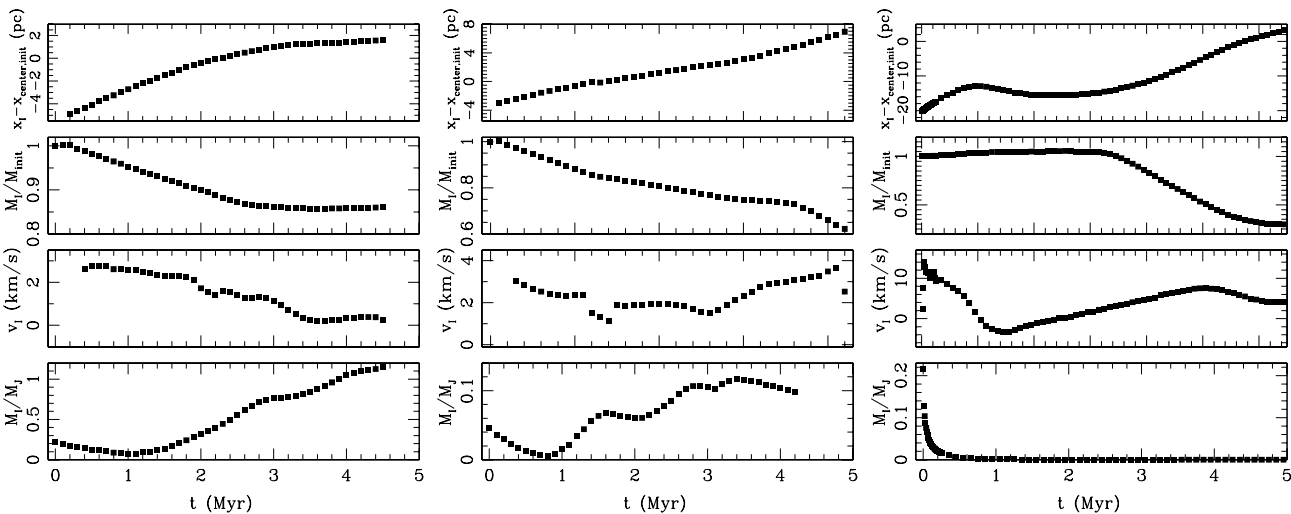


Figure 2. Evolution of (top to bottom panels): the position of the I-front along x-axis, x_I , the neutral mass fraction remaining in the clump, M_I/M_{init} , the velocity of the I-front v_I , and the ratio of the cold, neutral mass to the current (averaged) Jeans mass, M_I/M_J , for Cases 1 (left), 2 (middle) and 3 (right).

this paper, we assume the Galactic dust-to-gas ratio to be 0.01. We define the normalized dust-to-gas ratio κ as

$$D = \kappa D_{\odot}, \quad (5)$$

where D_{\odot} is the Galactic dust-to-gas ratio (i.e., $D_{\odot} = 0.01$), thus we assume $\kappa = 0.1$ and hence $D = 10^{-3}$.

The typical Galactic ISRF intensity has been estimated to be $cu_{\nu} = 1.2 \times 10^{-3} \text{ erg cm}^{-3}$ at the wavelength of 1000 \AA (i.e., $\nu = 3.0 \times 10^{15} \text{ Hz}$), where u_{ν} is the energy density of photon per unit frequency (Habing 1968). Approximating the energy density of photons at 1000 \AA with that at the Lyman-Werner Band, we obtain J_{LW} at the solar vicinity, $J_{\text{LW}\odot}$, is approximately $J_{\text{LW}\odot} \simeq cu_{\nu}/4\pi = 3.2 \times 10^{-20} \text{ erg cm}^{-2} \text{ s}^{-1} \text{ Hz}^{-1} \text{ sr}^{-1}$. The intensity normalized by the Galactic ISRF, χ , is introduced by

$$J_{\text{LW}} \equiv \chi J_{\text{LW}\odot}. \quad (6)$$

Using equations (3) and (6), we obtain

$$R_{\text{diss}} = 4.4 \times 10^{-11} \chi S_{\text{shield}} \text{ s}^{-1}. \quad (7)$$

When $\chi = 1$, the typical Galactic photodissociation rate ($2\text{--}5 \times 10^{-11} \text{ s}^{-1}$) derived by Jura (1974) is recovered.

The *UV* background intensity at the Lyman limit is taken to be $J_{21} = 0.3\text{--}1$ around $z \sim 3$, where J_{21} is in units of $10^{-21} \text{ erg cm}^{-2} \text{ s}^{-1} \text{ Hz}^{-1} \text{ sr}^{-1}$ (Giallongo et al. 1996; Cooke, Espey, & Carswell 1997; Scott et al. 2000; Bianchi, Cristiani, & Kim 2001). For the *UVB*, we assume that $J_{21} = 0.6$ and that the spectrum of ionizing radiation is described with a power law with slope of 1.55. We also take into account a ‘‘boost’’ of $10^{1.5}$ of the Lyman-Werner photons flux with respect to the ionizing flux at the threshold, according to the results of Haardt & Madau (1996) at $z = 2\text{--}4$ (i.e. we assume $\chi = 0.6$).

The *UV* radiation field originating from stars within DLAs may be larger than the *UVB* (Wolfe et al. 2003; Hirashita & Ferrara 2005). In particular, the *UVB* intensity is likely to be lower at $z \lesssim 1$ than at $z \sim 3$ (e.g. Scott et al. 2002). Therefore, we also examine the case where the *UV* field is dominated by internal stars. Hirashita & Ferrara (2005) have derived $\chi = 3\text{--}30$ by using observational data of H_2 -detected DLAs. We adopt $\chi = 15$ in this paper. Although it is known that ionizing photons are strongly absorbed

Table 1. Simulation parameters

Quantity	Case 1	Case 2	Case 3
spectrum	BB 5e4	BB 5e4	PL, $\alpha = 1.55$
r_{clump} (pc)	5	3	5
n_{clump} (cm^{-3})	30	30	30
n_{out} (cm^{-3})	0.3	0.3	0.3
T_{clump} (K)	100	100	100
T_{out} (K)	10^4	10^4	10^4
J_{21}	6	6	0.6
M_{cloud} (M_{\odot})	474	102	474
$f_{\text{H}_2, \text{init}}$	10^{-8}	10^{-8}	10^{-8}

by the neutral hydrogen within DLAs, there is little quantitative constraint on the intensity of ionizing photons.

However, it would be reasonable to assume that 90%–99% (Ciardi, Bianchi, & Ferrara 2002) of the ionizing photons are absorbed relative to the dissociating photons in passing through the interstellar medium, the “boost” could be 10–100. Assuming the boost of 50, we obtain $J_{21} = 6$ for the internal source. The spectral shape of the 50,000 K black-body is assumed for the internal source.

In summary, in our simulations we fix the value of the external ionizing flux entering the computational box, F , to be equivalent to a mean isotropic background J of either $J_{21} = 6$, with 50,000 K black-body spectrum for the cases where the ionizing sources and internal, nearby hot stars, or of $J_{21} = 0.6$, with power-law spectrum with slope of 1.55, for the mean intergalactic background (or possibly internal/nearby QSO sources). The level and spectrum of the ionizing flux $F(i, j)$ reaching each computational cell (i, j) is determined self-consistently by the code based on the optical depth from the source to the cell. Finally, the intensity in the Lyman-Werner bands (normalized to the Galactic value), χ , is assumed to be 0.6 for the UVB and 15 for the internal sources.

As mentioned at the beginning of this subsection, we can assume that the formation and destruction of H_2 are in equilibrium. Therefore, the following equation holds:

$$R_{\text{dust}} n n_{\text{H}} (1 - f_{\text{H}_2}) = R_{\text{diss}} n_{\text{H}_2}. \quad (8)$$

Using equation (8), the molecular fraction is obtained as:

$$f_{\text{H}_2} \equiv \frac{2n_{\text{H}_2}}{n_{\text{H}}} = \frac{2R_{\text{dust}} n}{R_{\text{dust}} n + R_{\text{diss}}}. \quad (9)$$

3 RESULTS

We have performed three high-resolution simulations with varying cloud sizes and external ionizing flux level and spectrum, summarized in Table 1. Cloud sizes and densities were chosen similar to the ones found on small scales in the larger-scale simulations of a galactic disk performed by Hirashita et al. (2003). In Figure 1 we show the density and size distribution functions of the clouds from the simulations in Hirashita et al. (2003), where each cloud is identified as a 2-D region with local gas density exceeding 10 cm^{-3} and the cloud radius is defined as $(A/\pi)^{1/2}$ (A is the area of the cloud).

In all cases of our simulations listed in Table 1, both the clump and the external medium start neutral, and the clumps are

in a pressure-supported equilibrium. Our fiducial case (Case 1) is a spherical cloud of radius $r = 5 \text{ pc}$, temperature $T = 100 \text{ K}$ and gas number density of $n = 30 \text{ cm}^{-3}$ (corresponding to a total clump mass of $M = 474 M_{\odot}$), and surrounding medium with temperature $T = 10^4 \text{ K}$ and gas number density of $n = 0.3 \text{ cm}^{-3}$. The external flux has 50,000 K black-body spectrum and $J_{21} = 6$. Our Case 2 simulation has all the same initial conditions as Case 1, except the clump is smaller, with initial radius of 3 pc (corresponding to a total clump mass of $M = 102 M_{\odot}$). Finally, we considered a case with power-law external ionizing flux, $f \propto \nu^{-\alpha}$ with a slope of $\alpha = 1.55$ and $J_{21} = 0.6$, and all other initial conditions the same as in Case 1. The Lyman-Werner flux is fixed in all cases by $J_{\text{LW}} = 474 J_{21}$, as described in the previous section.

The Inverse Strömgren length, ℓ_S , i.e. the size along a line-of-sight of the inverse static Strömgren volume from the source side into the clump gas along the axis of symmetry, is given by

$$\ell_S = \frac{F}{\alpha_{\text{H}}^{(2)} n_{\text{H}}^2}, \quad (10)$$

where $\alpha_{\text{H}}^{(2)}$ is the Case B recombination coefficient for hydrogen [see Shapiro, Iliev & Raga (2004) for details]. Numerically it is equal to $\ell_S = (0.005, 0.005, 0.0005) \text{ pc}$ in our Cases 1, 2 and 3, respectively, much smaller than the corresponding cloud diameter. Therefore the I-front would always convert to slow, D-type and become trapped by the cloud.

Cases 1 and 2 were run with 1024×2048 finest grid resolution, while Case 3 with 512×1024 , since simulations which adopt harder ionizing spectra converge more readily (Iliev, Shapiro, & Raga 2005), and thus do not require such high resolution. We have also tested our results for convergence by running lower-resolution simulation of Case 1, at 512×1024 finest-grid resolution. Our results show almost no dependence on resolution; thus our conclusions remain unchanged and unaffected by resolution concerns.

We show the evolution of the I-front position, velocity, and the neutral mass fraction remaining in the clump for Cases 1, 2 and 3 in Figure 2. We note that there are significant differences in the evolution of these quantities in the three cases. In Case 1 about 15% of the cloud mass becomes evaporated within the first 3 Myr after the arrival of the I-front, and no mass is lost afterward, with the cloud retaining the rest, about 85%, of its initial mass. The I-front initially propagates into the cloud with $v_I \sim 2 \text{ km s}^{-1}$. After that, its velocity continually decreases until the I-front stalls at $t \sim 3 \text{ Myr}$. The cloud itself is also moving during that time at $\sim 0.1 - 0.2 \text{ km s}^{-1}$, a manifestation of the well-known rocket effect, whereby the photoevaporating gas pushes the cloud away from the source due to conservation of momentum. In Case 2 the evolution is initially similar to the one observed in Case 1, with the cloud losing $\sim 25\%$ of its initial mass in the first 3 Myr due to photoevaporation with a subsequent decrease in the mass loss rate. However, in this case the outflow still continues afterward, albeit at a low level (the sharp decrease of the neutral mass fraction after 3.5 Myr is largely due to the cloud partially leaving the box, rather than to mass outflow, as would be seen below). The clump is again pushed away from the source due to rocket effect, at somewhat larger speed ($\sim 2 \text{ km s}^{-1}$). Finally, in Case 3 the cloud stays neutral for large part of its evolution, expanding into the surrounding gas until it eventually becomes mostly ionized between 3 Myr and 7 Myr after the arrival of the ionization front and disperses.

These cloud collapse/dispersion timescales due to radiative feedback, which are of order 3–7 Myr, are similar to the formation/survival timescales obtained from the gas-dynamic simula-

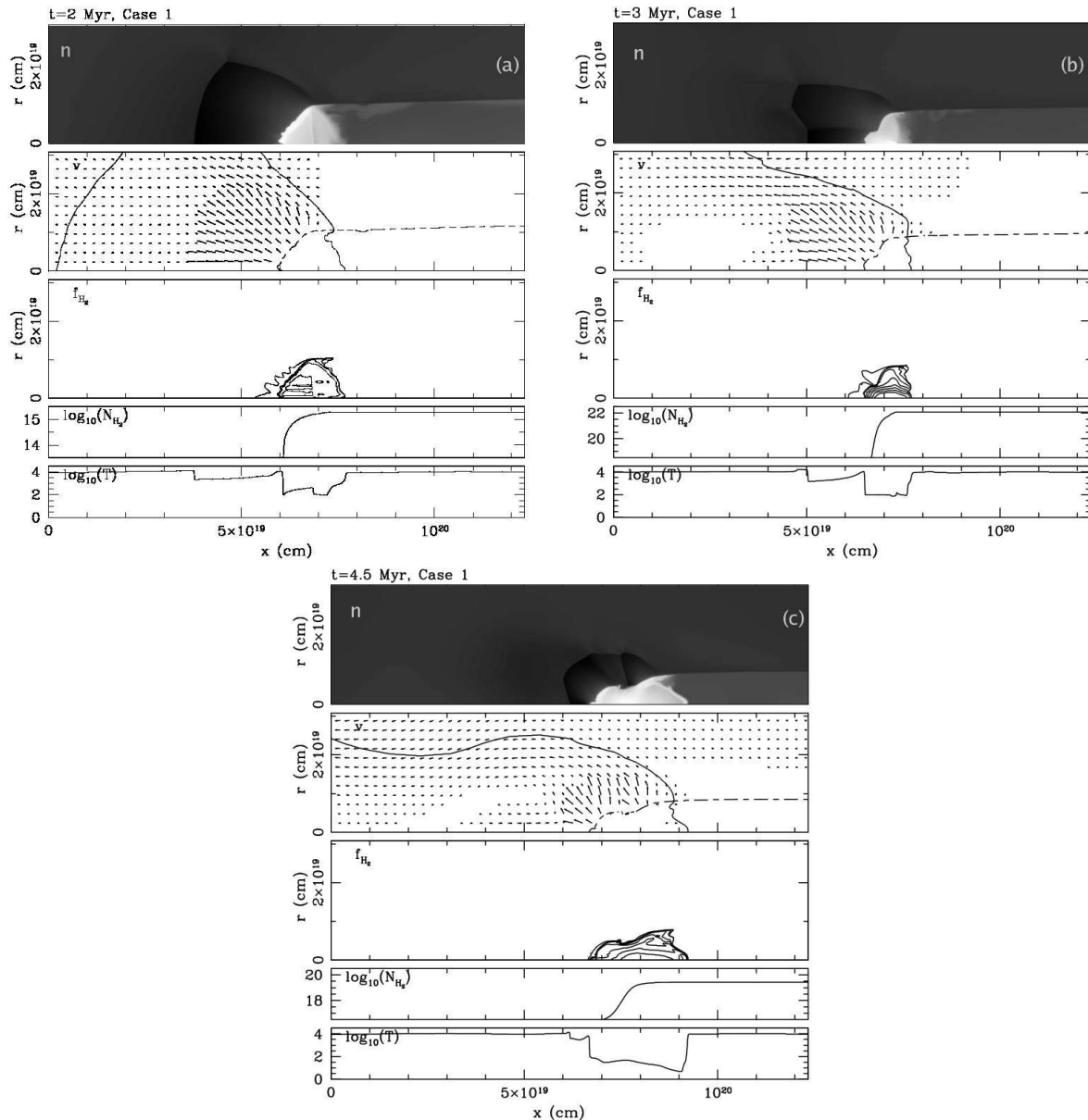


Figure 3. Case 1 simulation results at (a) $t = 2$ Myrs, (b) $t = 3$ Myrs and (c) $t = 4.5$ Myrs. From top to bottom: (1) grayscale image of the decimal logarithm of the atomic density in (r, x) -plane of cylindrical coordinates; (2) flow velocities; arrows are plotted with length proportional to gas velocity. An arrow of length equal to the spacing between arrows has velocity 25 km s^{-1} (i.e. arrows are touching along x - and y -axes if $v = 25 \text{ km s}^{-1}$); the minimum velocities plotted are 3 km s^{-1} . Solid line indicates the boundary of the gas which was originally inside the cloud, dashed line indicates the current position of the ionization front (50% ionization of H); (3) isocontours of H_2 fraction, f_{H_2} , logarithmically-spaced (from 1 down by factors of 10); cuts along the $r = 0$ axis of: (4) molecular hydrogen column density, N_{H_2} , (cm^{-2}) and (5) temperature (K).

tions in Hirashita et al. (2003), which can be roughly estimated as $t_{\text{survive}} \sim r_{\text{cloud}}/v_{\text{flow}} \approx 5 \text{ pc}/1 \text{ km s}^{-1} = 5 \text{ Myr}$, where v_{flow} is a typical gas flow velocity observed in the simulations. In the following, we discuss in more detail each of the Cases.

3.1 Case 1

Figure 3 shows snapshots of the gas flow for Case 1 at $t = 2, 3$ and 4.5 Myr. When the I-front reaches the clump (at time a fraction of a Myr) it slows down considerably, converts to D-type and gets trapped. Initially, as the I-front is entering the clump, some Raleigh-Taylor instabilities develop at the boundary between the

hot gas outside and the cold gas inside. The I-front is clearly preceded by a (oblique) shock (at the x -axis it is at $x \sim 6 \times 10^{19} \text{ cm}$ at time $t = 2$ Myr), as expected for a D-type I-front. A fraction of the cloud material is photoheated and evaporated, outflowing in a supersonic wind with speeds $\sim 25 \text{ km s}^{-1}$. The rest of the clump gas is strongly compressed by the propagating shocks. The dense, shocked neutral gas has sufficient column density to partially shield the unshocked part of the cloud and the hydrogen is already almost fully-molecular $f_{\text{H}_2} \sim 1$ there, while the H_2 column density through the cloud, N_{H_2} , exceeds 10^{19} cm^{-2} , and the molecular hydrogen self-shields. By $t = 2.5$ Myr the right-propagating shock which precedes the I-front crosses the whole clump. At $t = 3$ Myr

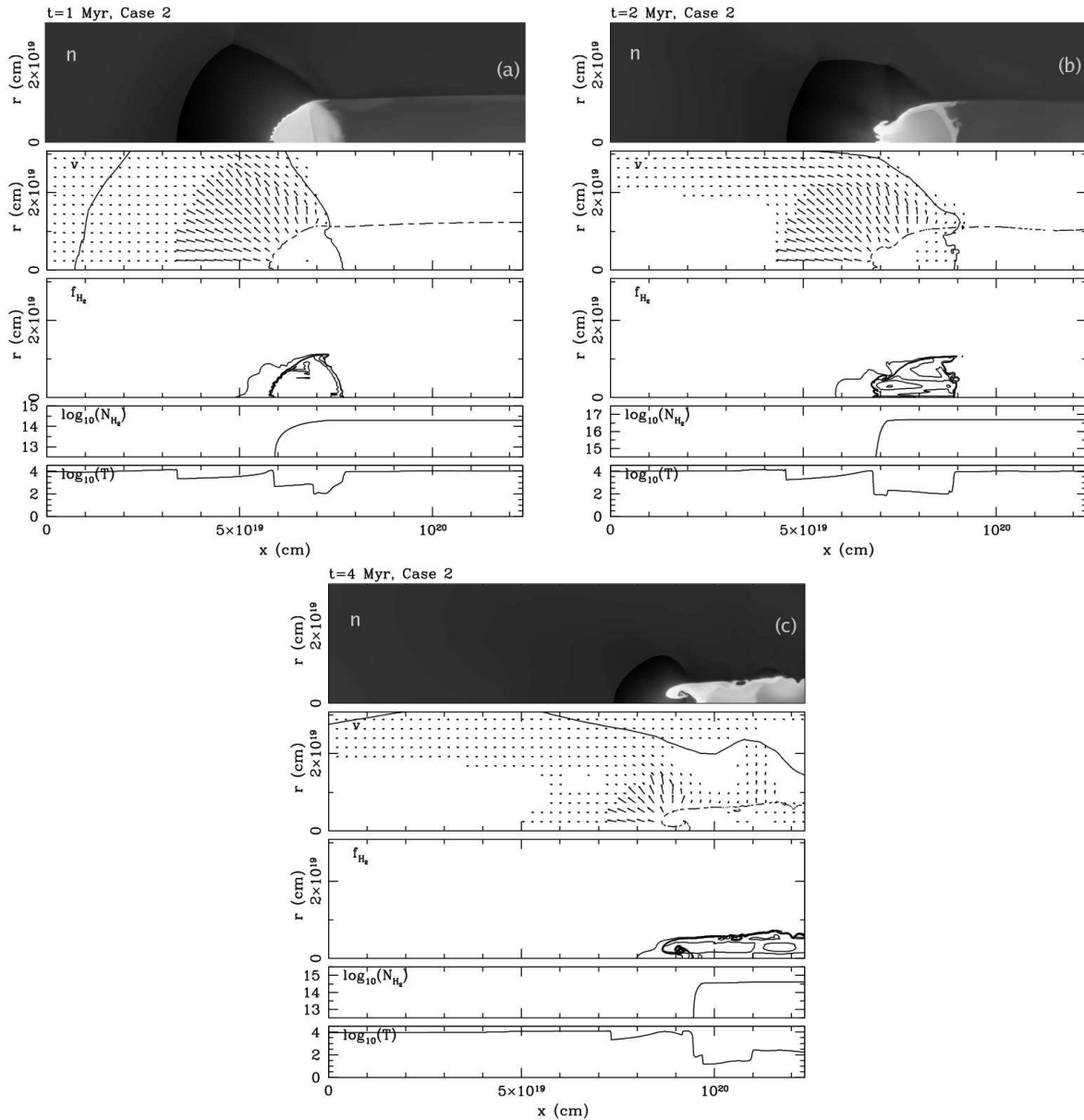


Figure 4. Same as in Fig. 3, but for Case 2 at times (a) $t = 1$ Myr, (b) $t = 2$ Myr, and (c) $t = 4$ Myr.

(Figure 3, (b)) the clump is compressed to less than a third of its original radius, and corresponding gas densities $n \gtrsim 10^3 \text{ cm}^{-3}$. By this time the neutral portion of the cloud is fully self-shielded and the hydrogen is completely molecular ($f_{\text{H}_2} \sim 1$) there, while the column density of H_2 , N_{H_2} , exceeds 10^{22} cm^{-2} . By $t = 4.5$ Myr the photoevaporation wind almost disappears, with the neutral mass of the cloud remaining stable. The clump is again close to uniform at this time, but compressed to a fraction of its original volume and gas number density of $n \sim 10^3 \text{ cm}^{-3}$. The clump remains self-shielded, contains about 85% of its original gas, and the hydrogen inside is largely in molecular form. The Jeans mass is given by

$$M_J = \left(\frac{k_B}{Gm_p} \right)^{3/2} \frac{T^{3/2}}{\rho^{1/2}}, \quad (11)$$

where k_B is the Boltzmann constant and G is the gravity constant and ρ is the gas mass density. In Figure 2 we plot the ratio of the

mass of the cold, neutral gas remaining to the mean Jeans mass at that time for all three simulations. The average Jeans mass is calculated based on the mass-weighted temperature and the mean gas density. For the compressed cloud ($t \sim 4$ Myr) we have approximately $T \approx 100$ K and $n \approx 500 \text{ cm}^{-3}$, and $M_J \approx 377 M_\odot$, while the mass of the neutral gas in the cloud at this point is about $400 M_\odot$, hence the cloud should become Jeans-unstable (see Fig. 2). Later on ($t \sim 4.5$ Myr) the cloud expands and the density drops slightly, but the temperature also drops due to adiabatic cooling to $T \sim 60$ K, and the local Jeans mass decreases a bit more. The physical conditions reached suggest the cloud becomes gravitationally-unstable, cold and molecular, which should lead to increased star formation in this case, triggered by the original I-front.

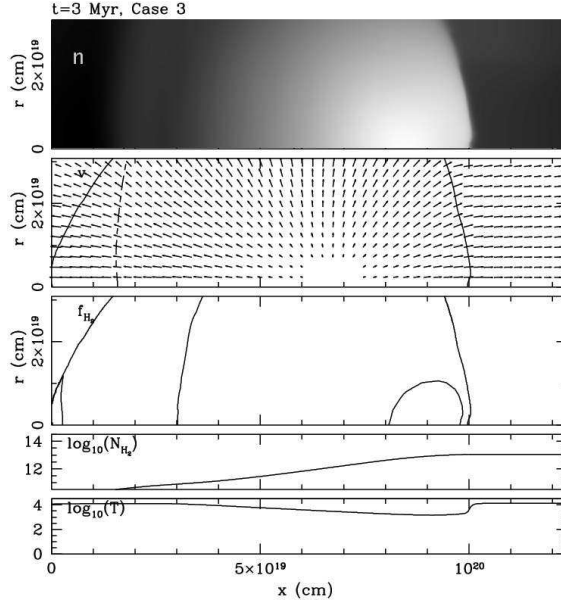


Figure 5. Same as in Fig. 3, but for Case 3 at $t = 3$ Myr.

3.2 Case 2

Results from our Case 2 at $t = 1, 2$ and 4 Myr are shown in Figure 4. In this case again the I-front is trapped in the cloud and converted to a D-type, preceded by a shock, and expanding a supersonic wind into the surrounding gas, as is clearly seen in Figure 4. At $t \sim 1$ Myr, some molecular hydrogen is created in the pre-shock part of the clump, but its fraction is very small, less than 10^{-4} . N_{H_2} reaches $\sim 10^{17.5} \text{ cm}^{-2}$, and the cloud self-shields.

The shocks again compress the cloud, similarly to Case 1, but the maximum gas number density reached in the course of the evolution is somewhat lower than in Case 1, never exceeding 10^3 cm^{-3} (Figure 4). At $t \sim 3$ Myr the clump reaches maximum density and the molecular fraction is $f_{\text{H}_2} \sim 1$, while N_{H_2} reaches maximum of $\sim 10^{20.5} \text{ cm}^{-2}$, becoming completely self-shielded.

Afterward, the gas outflow due to photoevaporation continues, albeit at a somewhat diminished level and the remaining cloud is accelerated. As the cloud is pushed back it expands and elongates, and its density decreases to $n \sim 10^2 \text{ cm}^{-3}$. By $t = 4$ Myr much of the molecular hydrogen is exposed to the radiation again and mostly destroyed, with f_{H_2} decreasing to less than 10^{-2} everywhere, while N_{H_2} decreases to $\sim 10^{18} \text{ cm}^{-2}$, however the cloud is still self-shielded.

At the point of maximum compression its density and temperature are $n \sim 10^3 \text{ cm}^{-3}$ and $T \sim 100$ K, respectively, and the local Jeans mass exceeds the mass of neutral gas remaining in the cloud. After the cloud expands again ($t \sim 4$ Myr) its density drops to $n \sim 10^2 \text{ cm}^{-3}$ and its temperature drops to $T \sim 60$ K, in which case the Jeans mass becomes $M_J \sim 600 M_\odot$, while the neutral gas remaining in the cloud is $M \sim 70 M_\odot$, i.e. it never becomes gravitationally-unstable (see Fig. 2). While the cloud is still self-shielded at that time, the hydrogen molecule fraction is low: and conditions are not conducive to star-formation in this case.

3.3 Case 3

The results for Case 3 are illustrated in Figure 5. The evolution in this case is quite different from the previous two cases. The I-

front is initially trapped outside the clump itself, but the hard photons which are present in this case reach the cloud, since they have much longer mean free path and start heating it. The cloud becomes heated to $T \sim 10^3 - 10^4$ K and never gets strongly compressed, but instead expands almost uniformly in all directions due to the higher pressure inside it. It eventually evaporates completely and never forms significant molecular hydrogen fraction.

3.4 Comparison with observations

Recent observations have revealed that DLAs host star formation activity (e.g., Wolfe et al. 2003). We have found that propagating I-fronts produced by internal stellar sources can trigger cooling instability (i.e. a “compression-cooling-further compression” cycle) and collapse of average clumps (with $r \gtrsim 5$ pc and $n \sim 30 \text{ cm}^{-3}$) in DLAs. The hydrogen in the collapsed clumps is largely in molecular form and the temperature stays below 100 K. The physical conditions are, therefore, favourable for star formation. This star formation is triggered by the gas compression due to the passage of the I-front. Hence, the UV produced by internal stellar sources works as a “positive feedback” for the star formation in DLAs. Based on our calculation, we propose that star formation in DLAs can trigger further star formation in dense clumps inside the DLA.

When this cooling instability is triggered by the passing I-front, as the cloud collapses its H_2 column density can temporarily reach very high values, up to 10^{22} cm^{-2} for clouds with $r \sim 5$ pc. However, this phase is quite short-lived and the cloud rebounds and re-expands moderately within less than 1 Myr. Due to this short timescale and the very small cross-section of the clouds, we do not expect that such phase would be easily observable. On the other hand, smaller clouds, with initial radii $\lesssim 4$ pc, also collapse but never reach H_2 column densities above $\sim 10^{18} \text{ cm}^{-2}$ and most of the hydrogen is not in molecular form.

Here we theoretically estimate the star formation rate of a DLA by using the cloud data from the simulation by Hirashita et al. (2003) shown in Figure 1. There are $N_A = 1092$ clouds of

$r > 4$ pc per each kpc^2 in this simulation, corresponding to mean spacing between the clouds of $\bar{x} = 10^3/N_A^{1/2} = 30.3$ pc and mean volume per cloud of $\bar{V} = \bar{x}^3 = 2.8 \times 10^4 \text{ pc}^3$. The total volume of the disk simulated in Hirashita et al. (2003) is $V_{\text{tot}} = 0.785 \text{ kpc}^2 \times 100 \text{ pc} = 7.9 \times 10^7 \text{ pc}^3$, corresponding to total number of clouds $N_{\text{tot}} = V_{\text{tot}}/\bar{V} \approx 2800$. Assuming a 4 pc cloud, and that 85% of the gas initially in the clump is converted into stars on a time-scale of 3 Myr, as our simulations indicate, this corresponds to a star formation rate per cloud $\text{SFR}_{\text{cl}} = 0.85M_{\text{cloud}}/3 \text{ Myr} \approx 70 M_{\odot}/\text{Myr}$, and total SFR of $\text{SFR} = \text{SFR}_{\text{cloud}}N_{\text{tot}} \sim 0.25 M_{\odot} \text{ yr}^{-1} \text{ kpc}^{-2}$. This star formation activity produces a local *UV* field. Hirashita & Ferrara (2005) related the surface density of SFR, Σ_{SFR} , and the *UV* field normalized to the Galactic value, χ , as follows

$$\Sigma_{\text{SFR}} = 1.7 \times 10^{-3} \chi M_{\odot} \text{ yr}^{-1} \text{ kpc}^{-2}. \quad (12)$$

Therefore, the SFR derived above produces a strong *UV* field corresponding to $\chi = 146$. The SFR estimated above is significantly higher than the value derived from recent observations of $0.01 - 0.05 M_{\odot} \text{ yr}^{-1} \text{ kpc}^{-2}$ (Wolfe et al. 2003; Hirashita & Ferrara 2005). The assumption that all the clouds collapse at the same time could be unrealistic, and in reality, the star formation activity in DLAs could be regulated. On the other hand, the external *UV* background, acts as a negative feedback in terms of star formation, as in our Case 3. Thus, we propose that the star formation activity in DLAs is quiescent (i.e. not starburst-like evolution) and strongly regulated by a combination of their internal radiative feedback and the external *UVB* field.

In Cases 1 and 2, the velocity dispersion within the H_2 -rich regions is a few km s^{-1} or less, consistent with the values derived from H_2 -detected components (Ledoux et al. 2003). The evaporating flow of ionized hydrogen produces a typical velocity width of $\sim 20 \text{ km s}^{-1}$. The coexistence of molecular clouds and evaporating flows may be the reason for the observed complex velocity structures in H_2 -detected components (e.g. Petitjean et al. 2002).

At the interface of molecular clouds and evaporating flows, H_2 suffers *UV* radiation and it is excited by *UV* pumping. This can be the reason for the observed high excitation temperature observed for H_2 rotational levels $J \gtrsim 2$ (Hirashita & Ferrara 2004 and references therein). We predict that highly excited H_2 has a higher velocity dispersion than H_2 in low excitation levels, qualitatively explaining some observations (e.g., an absorption system at $z = 2.595$ in the sight line of Q 0405–443; Ledoux et al. 2003).

4 SUMMARY AND CONCLUSIONS

We have examined if star formation activity in damped $\text{Ly}\alpha$ clouds (DLAs) can be triggered in the presence of *UV* radiation. We have performed high-resolution hydrodynamics and radiative transfer simulations of the effect of radiative feedback from propagating ionization fronts on high-density clumps. We have considered two sources of *UV* radiation field to which high-redshift ($z \sim 3$) galaxies could be exposed: one corresponding to the *UV* radiation originating from stars within the DLA, itself, and the other corresponding to the *UV* background radiation. We have found that, for clouds with a radius $r \gtrsim 4$ pc, the propagating I-fronts created by local stellar sources can trigger cooling instability and collapse of significant part, up to 85%, of the cloud, creating conditions for star formation in a timescale of a few Myr. The passage of the I-front also triggers collapse of smaller clumps (with $r \lesssim 4$ pc), but in

these cases the resulting cold and dense gas does not reach conditions conducive to star formation. Assuming that 85% of the gas initially in the clump is converted into stars in clouds with $r > 4$ pc, and using the statistics of the clouds in the simulation of an entire galactic disk by Hirashita et al. (2003), we obtain a surface density of star formation rate of $\sim 0.25 M_{\odot} \text{ yr kpc}^{-2}$. This is significantly higher than the value derived from recent observations. On the other hand, the background *UV* radiation which has harder spectrum fails to trigger cooling and collapse. Instead, the hard photons which have long mean-free-path heat the dense clumps, which as a result expand and essentially dissolve in the ambient medium. Therefore, the star formation activity in DLAs is strongly regulated by the radiative feedback, both from the external *UV* background and internal stellar sources and we predict quiescent evolution of DLAs (not starburst-like evolution). We believe these conclusions are fairly generic and are applicable also to molecular clouds in other types of galaxies, as long as the environmental conditions are similar, in particular in terms of significant presence of metals and dust.

ACKNOWLEDGMENTS

We thank the referee for helpful comments which improved our presentation. We are very grateful to Alejandro Raga and Garrelt Mellema for allowing us to use and modify their code CORAL. This research was partially supported by the Research and Training Network "The Physics of the Intergalactic Medium" set up by the European Community under the contract HPRN-CT2000-00126 RG29185. HH is supported by the University of Tsukuba Research Initiative.

REFERENCES

- Abel, T., Anninos, P., Zhang, Y., Norman, M. L. 1997, *NewA*, 2, 181
- Arthur S. J. 1991, PhD Thesis, University of Leeds
- Ciardi, B.; Bianchi, S.; Ferrara, A. 2002, *MNRAS*, 331, 463
- Cen, R., Ostriker, J. P., Prochaska, J. X., & Wolfe, A. M. 2003, *ApJ*, 598, 741
- Bianchi, S., Cristiani, S., & Kim, T.-S. 2001, *A&A*, 376, 1
- Cooke, A. J., Espey, B., & Carswell, R. F. 1997, *MNRAS*, 284, 55
- Draine, B. T., & Bertoldi, F. 1996, *ApJ*, 468, 269
- Ge, J., & Bechtold, J. 1997, *ApJ*, 477, L73
- Giallongo, E., Cristiani, S., D'Odorico, S., Fontana, A., & Savaglio, S. 1996, *ApJ*, 466, 46
- Haardt F. & Madau P. 1996, *ApJ*, 461, 20
- Habing H. J. 1968, *Bull. Astr. Inst. Netherlands*, 19, 421
- Haehnelt, M. G., Steinmetz, M., & Rauch, M. 1998, *ApJ*, 495, 647
- Hirashita, H., & Ferrara, A. 2002, *MNRAS*, 337, 921
- Hirashita, H., & Ferrara, A. 2005, *MNRAS*, 356, 1529
- Hirashita, H., Ferrara, A., Wada, K., & Richter, P. 2003, *MNRAS*, 341, L18
- Hollenbach, D. J., & McKee, C. F. 1979, *ApJS*, 41, 555
- Howk, J. C., Wolfe, A. M., & Prochaska, J. X. 2005, *ApJ*, 622, L81
- Iliev I. T., Shapiro P. R., & Raga, A. C., 2005, *MNRAS*, 361,405
- Jura, M. 1974, *ApJ*, 191, 375
- Lanzetta, K. M., Wolfe, A. M., & Turnshek, D. A. 1995, *ApJ*, 440, 435

- Ledoux, C., Petitjean, P., Bergeron, J., Wampler, E. J., & Srianand, R. 1998, *A&A*, 337, 51
- Ledoux, C., Petitjean, P., & Srianand, R. 2003, *MNRAS*, 346, 209
- Ledoux, C., Srianand, R., & Petitjean, P. 2002, *A&A*, 392, 781
- Lu, L., Sargent, W. L. W., Barlow, T. A., Churchill, C. W., & Vogt, S. S. 1996, *ApJS*, 107, 475
- Mellema G., Raga A. C., Canto J., Lundquist P., Balick B., Steffen W., & Noriega-Crespo A. 1998, *A&A*, 331, 335
- Omukai, K. 2000, *ApJ*, 534, 809
- Péroux, C., McMahon, R. G., Storrie-Lombardi, L. J., & Irwin, M. J. 2003, *MNRAS*, 346, 1103
- Petitjean, P., Srianand, R., & Ledoux, C. 2002, *MNRAS*, 332, 383
- Pettini M., Smith L. J., Hunstead R. W., & King D. L. 1994, *ApJ*, 426, 79
- Prochaska J. X., & Wolfe A. M. 1998, *ApJ*, 507, 113
- Prochaska J. X., & Wolfe A. M. 2002, *ApJ*, 566, 68
- Raga A. C., Mellema G., & Lundquist P. 1997, *ApJS*, 109, 517
- Raga A. C., Taylor S. D., Cabrit S., & Biro S. 1995, *A&A*, 296, 833
- Rao, S., & Briggs, F. 1993, *ApJ*, 419, 515
- Scott J., Bechtold J., Dobrzycki A., & Kulkarni V. P. 2000, *ApJS*, 130, 67
- Scott J., Bechtold J., Morita M., Dobrzycki A., & Kulkarni V. P. 2002, *ApJ*, 571, 665
- Shapiro P. R., Iliev I. T., Raga A. C., 2004, *MNRAS*, 348, 753
- Shibai, H., Okumura, K., & Onaka, T. 1999, in T. Nakamoto, ed., *Star Formation 1999*, Nobeyama, Nobeyama Radio Observatory, p. 67
- Srianand, R., Shaw, G., Ferland, G. J., Petitjean, P., & Ledoux, C. 2005, *MNRAS*, in press
- Storrie-Lombardi L. J., & Wolfe A. 2000, *ApJ*, 543, 552
- van Leer B. 1982, *Lect. Notes in Phys.*, 170, 507
- Wada, K., & Norman, C. A. 2001, *ApJ*, 546, 172
- Wolfe, A. M., Prochaska, J. X., & Gawiser, E. 2003, *ApJ*, 593, 215
- Wolfe, A. M., Turnshek, D. A., Smith, H. E., & Cohen, R. D. 1986, *ApJ*, 61, 249